International Journal of Biological Macromolecules 58 (2013) 23–30

Contents lists available at SciVerse ScienceDirect

International Journal of Biological Macromolecules

journal homepage: www.elsevier.com/locate/ijbiomac

Chitin-natural clay nanotubes hybrid hydrogel

Mingxian Liu[a,b], Yun Zhang[a], Jingjing Li[a], Changren Zhou[a,*]

[a] Department of Materials Science and Engineering, Jinan University, Guangzhou 510632, China
[b] Key Laboratory of Rubber-Plastics of Ministry of Education/Shandong Provincial Key Laboratory of Rubber-plastics, Qingdao University of Science & Technology, Qingdao 266042, China

ARTICLE INFO

Article history:
Received 15 January 2013
Received in revised form 15 February 2013
Accepted 16 March 2013
Available online xxx

Keywords:
Chitin
Halloysite
Hydrogel
Nanocomposites
Mechanical property
Absorption

ABSTRACT

Novel hybrid hydrogel was synthesized from chitin NaOH/urea aqueous solution in presence of halloysite nanotubes (HNTs) via crosslinking with epichlorohydrin. Fourier transform infrared (FT-IR) spectra and atomic force microscopy (AFM) results confirmed the interfacial interactions in the chitin–HNTs hybrid hydrogel. The compressive strength and shear modulus of chitin hydrogel were significantly increased by HNTs as shown in the static compressive experiment and rheology measurement. The hybrid hydrogels showed highly porous microstructures by scanning electron microscopy (SEM). The swelling ratio of chitin hydrogel decreased because of the addition of HNTs. The malachite green's absorption experiment result showed that the hybrid hydrogel exhibited much higher absorption rate than the pure chitin hydrogel. The prepared hybrid hydrogel had potential applications in waste treatment and biomedical areas.

1. Introduction

In recent years, special attention has been drawn to the development and application of biopolymers due to their good biocompatibility, favorable biodegradability, and abundant availabilities [1]. Chitin is a long-chain biopolymer of N-acetylglucosamine, which can be found in many sources throughout the natural world [2]. Chitin is the main component of the cell walls of fungi, the exoskeletons of arthropods such as crustaceans (e.g., crabs, lobsters and shrimps) and insects, the radulas of mollusks, and the beaks of cephalopods, including squid and octopuses. Due to its intrinsic biofriendly properties and abundant availabilities, chitin has been used for several medical and industrial purposes [3]. Because of strong inter/intra-molecular hydrogen bonding, chitin has high degree of crystallization and low solubility in common solvents, which limits its applications [4,5]. Strong acids and polar solvents such as trichloroacetic acid (TCA), dichloroacetic acid (DCA), hexafluoroisopropyl alcohol, and lithium chloride (LiCl)/dimethylacetamide (DMAc) mixtures etc. have been found to dissolve chitin. But these solvents show a low efficiency when dissolving chitin and the dissolution process is usually hard to handle. Until recently, Zhang et al. developed a new method to dissolve chitin in NaOH/urea aqueous solution via freezing/thawing process [6,7]. The urea in alkali solutions can break the hydrogen bondings among the chitin, leading to dissolution of chitin. This new method of dissolving chitin realizes the preparing of chitin hydrogel or aerogel from the transparent chitin aqueous solutions [8]. The prepared chitin hydrogel or aerogel find a vast range of applications, from drug delivery, tissue engineering, heat or sound insulators, to waste treatment materials. The direct dissolution of chitin with NaOH/urea systems, avoiding the deacetylation process (to obtain chitosan), is beneficial to amplify the application of the renewable chitin, which is also favorable to environment protection. Although the chitin hydrogel or aerogel has exhibited good mechanical strength, the mechanical performance should be further improved to expand their application areas so as to lower the cost of the materials.

One of the most promising solutions to enhance the mechanical and thermal performance of polymers is elaboration of nanocomposite or organic-inorganic hybrid materials, namely the uniform dispersion of nanosized filler into a polymer matrix [9,10]. Halloysite nanotubes (HNTs), one kind of natural nanoclays with unique tubular microstructure and high strength, can be employed to prepare the chitin nanocomposites or hybrid materials. HNTs, with a chemical formula of $Al_2Si_2O_5(OH)_4{\cdot}nH_2O$, are a dioctahedral 1:1 clay mineral that appear largely in soils, especially in wet tropical and subtropical regions and various weathered igneous and non-igneous rocks [11]. HNTs have dominantly hollow tubular structure in nano-scale with aspect ratio of ca. 20. The length of tubes ranges from 500 to 1500 nm, while the external diameter

* Corresponding author. Fax: +86 20 8522 3271.
E-mail address: tcrz9@jnu.edu.cn (C. Zhou).

0141-8130/$ – see front matter © 2013 Elsevier B.V. All rights reserved.
http://dx.doi.org/10.1016/j.ijbiomac.2013.03.042

from 40 to 70 nm and the inner diameter from 10 to 15 nm [12]. HNTs have found applications in many fields, such as bioreactor, time-release capsule, catalysts of polymer degradation, template, and high-tech ceramic applications. In recent years, HNTs have been evaluated as nanofillers for polymers [13]. Attributed to their excellent hydrophilicity and small dimension, HNTs are readily dispersed in water, which is convenient to prepare water-soluble polymers nanocomposites. For example, transparent polyvinyl alcohol (PVA)/HNTs and chitosan/HNTs nanocomposites films have been fabricated via solution casting method [14,15]. Uniformly dispersed nanotubes morphology is obtained in these hydrophilic polymers/HNTs nanocomposite systems. Also, HNTs/polymers nanocomposites exhibit a significant increase in mechanical and thermal properties owing to the good interfacial bonding and/or uniformly dispersed rigid nanotube in the composite systems [16]. As an alternative one-dimensional nanoparticle for carbon nanotubes, HNTs are cheap, abundantly available, environmental-friendly, mechanically strong and biocompatible [17]. Therefore, exploring HNTs for preparing bio-based, renewable and high performance chitin nanocomposites is significant both in theory and practice.

In the present study, chitin–HNTs hybrid hydrogels were successfully synthesized via solution mixing and then crosslinking with epichlorohydrin. Raw chitin was firstly dissolved in the NaOH/urea aqueous solution and then the chitin solution was mixed with HNTs. The chitin–HNTs hybrid hydrogel was prepared at elevated temperature using epichlorohydrin as a crosslinker. The interfacial interactions in the chitin–HNTs hybrid hydrogels were confirmed by Fourier transform infrared spectroscopy and atomic force microscopy. The compressive strength and shear modulus of chitin hydrogel were determined. The microstructure of the chitin–HNTs hybrid hydrogel was observed by scanning electron microscopy (SEM). The malachite green's absorption experiment showed that the hybrid hyrogel exhibits much higher absorption efficiency than pure chitin hydrogel. The relationship between the property of the chitin–HNTs hybrid hydrogel and their microstructures were correlated accordingly. Due to the high mechanical performance and unique structural features of the chitin–HNTs hybrid hydrogel, they had potential applications in waste treatment and biomedical areas.

2. Experimental

2.1. Materials

Chitin powder (K1262) was purchased from Sanland-chem International Inc. and used without further purification. The degree of acetylation (DA) of the chitin was determined by elemental analysis to be 0.98. The halloysites was mined from the deposit of the Hunan province, China, and used after purification according to the reference [12]. The raw HNTs showed a layer spacing of 7.2 Å indicating their high dehydration state. The elemental composition of the used HNTs was determined by X-ray fluorescence (XRF) as follows (wt.%): SiO_2, 58.91; Al_2O_3, 40.41; Fe_2O_3, 0.275; TiO_2, 0.071. The Brunauer–Emmett–Teller (BET) specific surface area was approximately 50.4 m^2/g. Epichlorohydrin (ECH) and malachite green (MG) (chemical formula: $(C_{23}H_{25}ClN_2)_2 \cdot C_2O_4 \cdot 2H_2C_2O_4$) were of analytical-grade and used without further purification.

2.2. Synthesize of the chitin–HNTs hybrid hydrogel

The chitin NaOH/urea solution was prepared according to Zhang's method [7]. The typical dissolution procedure was shown as follows. Chitin powders were dispersed into 8 wt% NaOH/4 wt% urea/88 wt% water mixture with stirring, and then were stored under refrigeration (−80 °C) for 4 h. Subsequently, the frozen solid was thawed and stirred extensively at room temperature. After three freezing/thawing cycles, transparent chitin solutions were obtained by centrifugation. The final concentration of the chitin solution was determined as 2 wt.%. Then the calculated HNTs powders were added into the chitin solution with stirring for 24 h to ensure the good dispersion and the absorption between them. Then 0.1 mL ECH was added as cross-linker to 1 g of the chitin solution and stirred at room temperature for 0.5 h to obtain a homogeneous solution. The solutions were casted into glass tubes with the diameter of 13 mm. The crosslinking reaction was carried out in a vacuum oven at 60 °C for 1 h and the hydrogels were obtained by breaking the glass. Pure chitin hydrogel (CT) was also prepared in the same conditions but without the addition of HNTs. The sample codes of the hybrid hydrogel (CT2N1, CT1N1, CT1N2, CT1N4) stood for the weight ratio of chitin (CT) and the nanotubes (N). For example, the CT1N2 stood for the weight ratio of chitin to HNTs was 1:2 in the hybrid hydrogel. The maximum of HNTs concentration was 80 wt.% (CT1N4), and further increasing the HNTs concentration in the chitin solution leaded not applicably high viscosity to process. All the prepared hydrogels were washed with distilled water to remove alkali, urea, and excess ECH before measurement. The prepared pure chitin hydrogel was transparent, while all the chitin–HNTs hybrid hydrogels were opaque (Fig. 1(a)). This may be due to the relatively large dimension of HNTs compared with the visible light wavelength.

2.3. Characterization

Atomic force microscopy (*AFM*) To evaluate the surface morphology of raw HNTs and chitin–HNTs, a multimode AFM with NanoScope IIIa controller was used (Veeco Instruments). The dilute HNTs dispersion and chitin–HNTs (1/1, w/w) solution were dispersed on a piece of freshly cleaved mica and images were collected under contact mode using a soft cantilever (NP-S20, Veeco, force constant ca. 0.1 nN/nm).

Fourier transform infrared spectroscopy (*FTIR*) FTIR of raw HNTs, ECH, and ECH treated HNTs were recorded in a Bruker FTIR using transmission mode by mixing the samples with KBr in an agate mortar and then pressed into pellets and scanned in transmission model. The FTIR spectra of pure chitin and chitin-HNTs freezing-dried gel were measured using attenuated total reflectance (ATR) model in a Bruker FTIR. ATR was a sampling technique used in conjunction with infrared spectroscopy which enabled samples to be examined directly in the solid without further preparation. Thirty-two consecutive scans were taken and their average was stored. Spectra were taken from 4000 to 400 cm^{-1}. The resolution of the wavenumber was 2 cm^{-1}.

Mechanical properties determinations Compression testing of chitin and chitin–HNTs hybrid hyrogels was carried out using Zwick/Roell Z005 machine under 25 °C. The samples for compression testing were cylinder samples with diameter of 10 mm and thickness of 10 mm. Tests were conducted with a constant strain rate of 2 mm/min and up to failure. The stress–strain curves for every sample were recorded automatically. At least five samples were used to obtained reliable data.

Rheological property measurements Rheological property measurements of the hydrogels were conducted with a Kinexus rotational rheometer (Malvern Instruments, Ltd.) using parallel plates of diameter of 20 mm at 25 ± 0.5 °C. The gap between the two parallel plates was set as 1 mm. Firstly, the dynamic strain sweep from 0.01 to 100% was carried out at angular frequency of 1 Hz. Then, the frequency sweep was performed over the frequency range of 0.001–100 Hz at the fixed strain of 0.5%.

Scanning electron microscopy (*SEM*) Before SEM observation, the freeze-dried hydrogels were sectioned and were sputter coated with 10 nm thick gold–palladium layer using a sputter coater

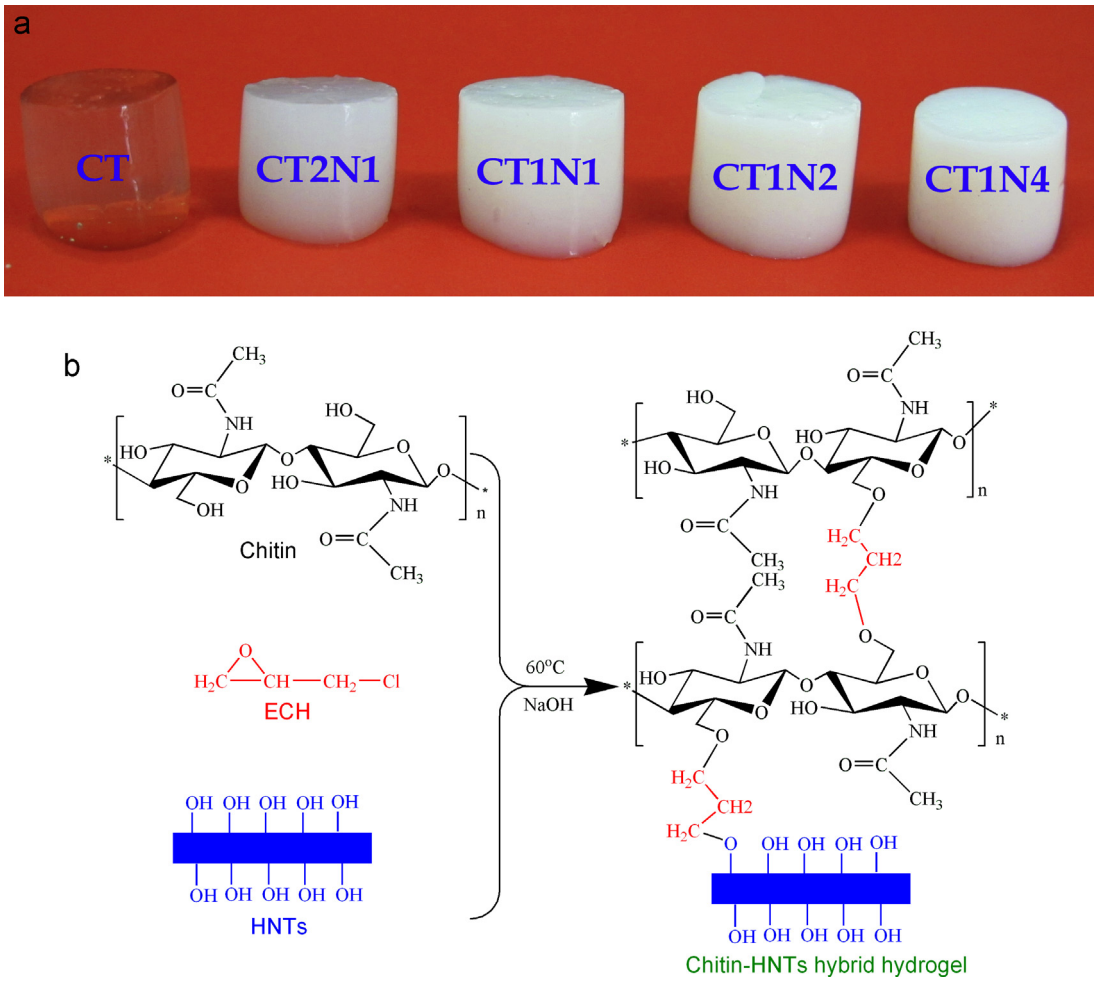

Fig. 1. Appearance (a) and reaction mechanism (b) of chitin and chitin–HNTs hybrid hydrogel.

(BALTEC SCD 005). The morphology of the scaffolds was observed with a Philips XL30 ESEM.

Swelling experiments Swelling experiments for all the samples were performed at room temperature by immersing the prepared hydrogels (initial size of 10 mm diameter × 5.0 mm length) in excess of pure water at room temperature, and changing the water for several times. The weight of the swollen hydrogel was recorded after 48 h. The equilibrium degree of swelling (EDS) was calculated by the following equation.

$$\text{EDS}\,(\%) = \frac{W_s - W_i}{W_i} \times 100$$

here, W_s was the weight of the swollen gel, W_i was the weight of the corresponding initial hydrogel.

Adsorption dye studies The experiment of determining the efficiency of the removal of MG from aqueous solutions by pure chitin hydrogel and chitin–HNTs hybrid hydrogel was performed by using different beakers containing around 10 g of hydrogel in 40 mL of the dye solution (0.8 mmol L^{-1}). The beakers were placed in shaker table with rate of 80 stroke/min under room temperature. At desired time intervals, the remaining amount of dye in the aqueous solution was determined by UV spectrophotometery by monitoring the absorbance changes at the wavelength of 325 nm. The amount of MG adsorbed on hydrogel was calculated by the following equation:

$$q_e = \frac{(c_o - c_e)V}{W}$$

where q_e was the amount of MG adsorbed onto the unit amount of the hydrogel (mmol g^{-1}), c_0 was the initial concentration of MG (mmol L^{-1}), c_e was the final or equilibrium concentration of MG (mmol L^{-1}), V was the volume of MG solution (L) and W was the weight of hydrogel (g).

3. Results and discussion

3.1. The formation and the interactions of the chitin–HNTs hybrid hydrogel

Previously, it was found that chitin aqueous solution could react with ECH at 60 °C to form a hydrogel [7]. The etherification between hydroxyl groups of chitin and the epoxy groups of ECH can occur at elevated temperature in the presence of NaOH solution. In the present study, in the chitin–HNTs mixture solution, the hydroxyl groups of HNTs could also interact with the ECH via etherification. The possibility of ECH to interact with HNTs was confirmed by FTIR spectra. Fig. 2(a) shows the typical FTIR spectra of HNTs and ECH, which is consistent with the standard spectral database [18]. A new peak around 1115 cm^{-1} assigned to the vibrations of Al—O—C or Si—O—C bond emerges in the HNTs treated with ECH samples [19], indicating the formation of covalent bond linking between HNTs and ECH. Also, the peak around 534 cm^{-1} assigned to the deformation of Al—O—Si for HNTs moves to 531 cm^{-1} in the ECH–HNTs. This shift is due to the formation of new Al—O—C or Si—O—C bond, which affects the energy of the Al—O—Si. Therefore,

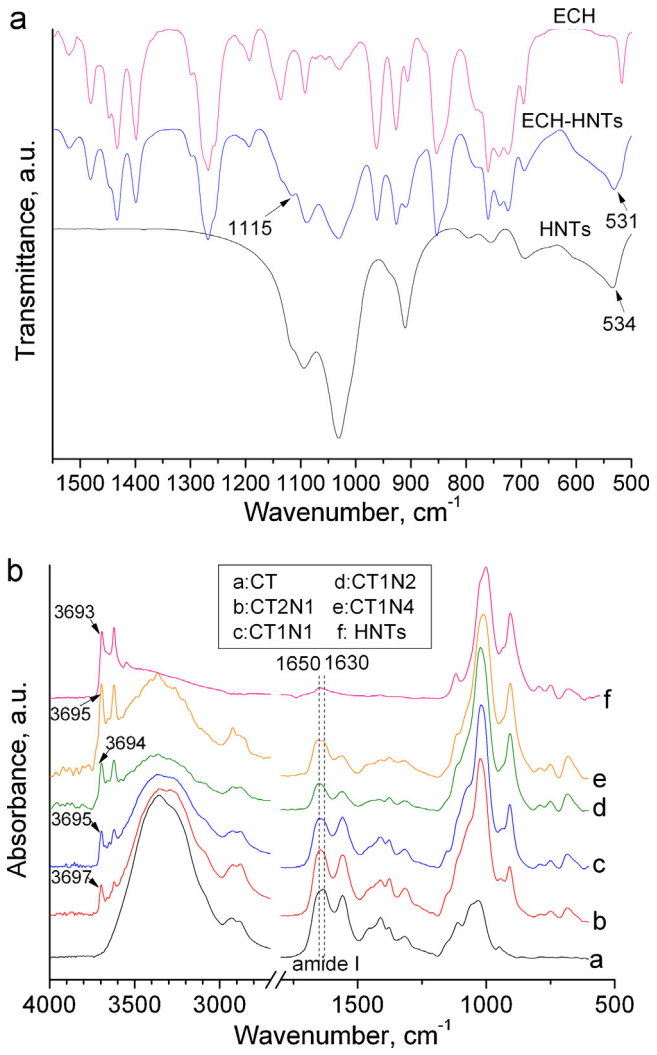

Fig. 2. FTIR of HNTs, ECH and ECH treated HNTs (a) and the chitin–HNTs dried gels (b).

the reactions between epoxy groups of ECH and hydroxyl groups of chitin–HNTs lead to formation of covalent bonding in the hybrid hydrogel. Fig. 1(b) illustrates the cross-linking reaction mechanism of the chitin–HNTs hybrid hydrogels. ECH is a highly efficient cross-linking agent both for chitin and HNTs, which forms covalent ether bridges between —OH groups of the chitin chains, as well as the hydroxyl groups located on HNTs sheets and particularly on their edges. The covalent bond of chitin and HNTs with ECH is responsible for the formation of hybrid materials and the enhanced properties as illustrated below. Other similar interfacial crosslinking reactions by small organic molecules for preparing organic–inorganic hybrids have also been reported [20,21].

Apart from the covalent bongding between chitin and HNTs, the hydrogen bonding interactions between them may also exist. The interactions between HNTs and chitin were reflected by FTIR (Fig. 2(b)). For chitin, the OH stretching band appears at 3450 cm^{-1}, amide I bands at 1655 and 1630 cm^{-1}, amide II band at 1560 cm^{-1}, C—H stretching band at 2877 cm^{-1}, the bridge oxygen stretching band at 1160 cm^{-1}, and the C-O stretching bands at 1070 and 1030 cm^{-1} [22]. For HNTs, the peak around 3695 cm^{-1} is attributed to the stretching of inner-surface hydroxyl groups, and the peak around 3620 cm^{-1} is attributed to the stretching of inner hydroxyl groups [11]. The intensity ratio of the absorbance at 1650 and 1630 cm^{-1} for the hybrid gel samples decreases compared with the pure chitin sample. This is due to the hydrogen bonding interactions between chitin and HNTs. Another evidence for the formation of hydrogen bonding is the slight shift of the peaks at 3693 cm^{-1} assigned to Al—OH groups of HNTs in the hybrid hydrogel. The FTIR result confirms the interfacial interactions in the hybrid hydrogel.

AFM result further confirms the interfacial interactions between chitin and HNTs. The morphology of raw HNTs is relatively uniform and the tubular quality of HNTs is good. From AFM images in Fig. 3, the walls of raw HNTs are clean and smooth. In contrast, the walls of chitin–HNTs are much rougher and the diameters of a tube are not uniform, indicating a polymer layer around the nanotubes. From high magnification AFM images and the R_q profiles of line scan, the diameter of the nanotubes in chitin-HNTs sample is larger than that of raw HNTs. For example, the diameter of a selected nanotube is 166 nm in raw HNTs sample, while it is 233 nm in the chitin–HNTs sample. The surface roughness (R_q) of the selected nanotube also increases from 57.7 mV of the raw HNTs to 93.0 mV of the chitin–HNTs. All these results suggest the presence of a chitin layer around the surfaces of the HNTs. The absorption of chitin chains on the HNTs is attributed to the hydrogen bonding interactions between them.

Table 1
Mechanical properties value of chitin and chitin-HNTs hybrid hydrogels (Data in the parentheses indicates the standard deviations).

Samples (wt.%)	Maximum stress kPa	Fracture strain %
Pure Chitin	23.1 (0.7)	78.9 (2.4)
CT2N1 (33.3% HNTs)	33.3 (0.5)	77.8 (4.3)
CT1N1 (50.0% HNTs)	40.2 (0.9)	71.0 (3.1)
CT1N2 (66.7% HNTs)	47.4 (1.2)	57.0 (1.8)
CT1N4 (80.0% HNTs)	59.2 (0.4)	55.3 (2.4)

3.2. Mechanical propeties of chitin–HNTs hybrid hydrogel

The pure chitin hydrogels are relatively weak [7], which hinders their applications where high stress is required. The weak mechanical performance of the hydrogels mainly arises from their low resistance to crack propagation and a lack of an efficient energy dissipation model in the network. To improve the mechanical properties, incorporation of nano-scaled reinforcement for preparing nanocomposite hydrogel is an effective method [10,23]. Fig. 4 shows the stress-strain curves for chitin and chitin–HNTs hybrid hydrogel. Table 1 summarizes the compression property data of chitin and chitin–HNTs hybrid hydrogel. All samples exhibit "J" shape curves, and the compressive stress increases slowly with an increase of strain and then rises abruptly. One can see that HNT have a significant effect on the mechanical properties of the chitin hydrogel. The fracture stress of the chitin–HNTs hybrid hydrogels significantly increases compared with the pure chitin hydrogel. Also, the increment in mechanical performance is proportional to the loading of HNTs in the hybrid hydrogel. The maximum compressive strength of the chitin–HNTs is ~60 kPa, which is ~300% higher than that of pure chitin hydrogel. However, the flexibility of the hybrid hydrogel is declining as the maximum fracture strain of the hybrid hydrogel decreases with the increase of HNTs. The decreased fracture strain may arise from the high inorganic clay loading in the hybrid hydrogel, since the inorganic phase has much lower elasticity compared with the soft polymer matrix. For example, apart from the water the CT1N4 sample has as high as 80 wt.% clay content, while the chitin content is only 20 wt.%. Also, this decreased fracture strain agrees with most of particles-filled polymer systems, as the strength and toughness of materials always have trade-off relationship [24]. From the mechanical property result, it can be concluded that the chitin-HNTs hybrid hydrogels exhibit a significant increase in mechanical strength compared with

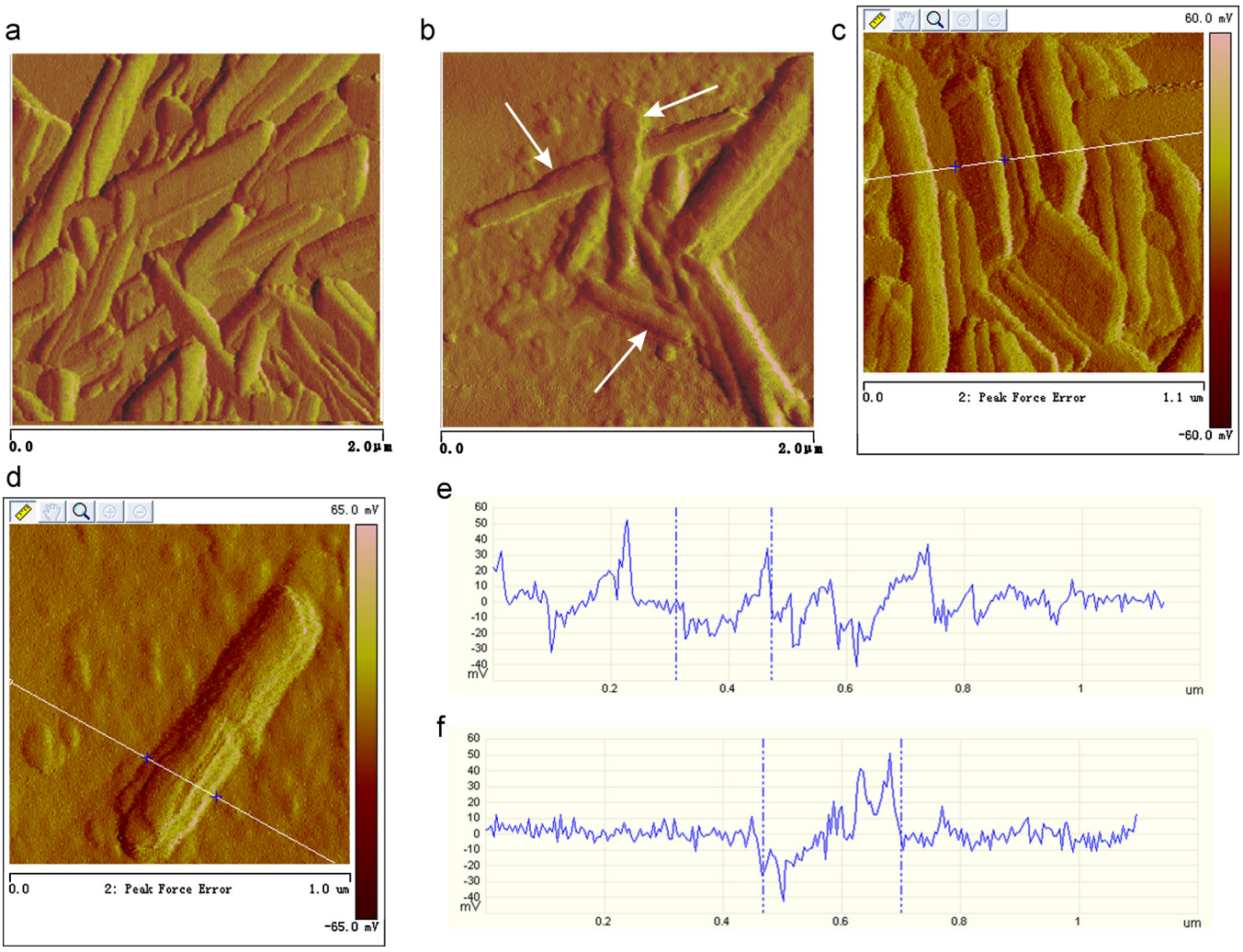

Fig. 3. AFM image of HNTs (a, c) and chitin-HNTs (b, d) and R_q profile of the line scan in (c) and (d). The arrows represent the location of chitin layers in the HNTs surfaces.

pure chitin and chitosan hydrogels, which is due to the reinforcing effect of HNTs to chitin and the interfacial interactions in the systems.

3.3. *Viscoelastic properties of chitin–HNTs hybrid hydrogels*

To further study the effect of HNTs on mechanical performance of chitin–HNTs hybrid hydrogel, dynamic viscoelasticity of chitin and chitin–HNTs hybrid hyrogels were examined in dynamic stress environment by rheometer. Fig. 5(a) shows the shear modulus (G′) curves of the chitin and chitin–HNTs hybrid hydrogels as a function of strain. The absolute values of the shear modulus for the hybrid hydrogels substantially increase with the loading of HNTs especially at high HNTs loadings, which is in consistent with the change of compressive mechanical properties above. For example, the G′ of CT1N4 hydrogel at 1% strain is 4827 Pa, which is 84.7 times higher than that of pure chitin hydrogel. The value of the shear modulus of pure chitin hydrogel and the hybrid hydrogels with relative low HNTs loading is nearly independent on strains over the range from 0.1 to 100%. However, for the hybrid hydrogels with relative high HNTs loading (CT1N2 and CT1N4), the shear modulus sharply decreases with the increasing of the strain. The difference among the samples may arise from the formation of two types of network structures in the hybrid hydrogel with high HNTs loading, i.e. the

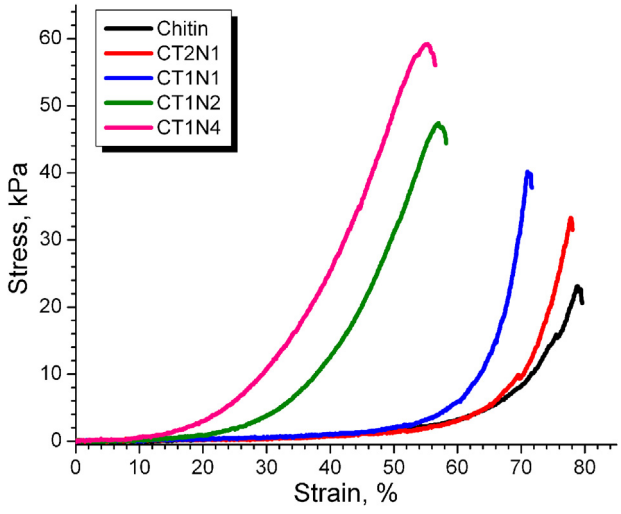

Fig. 4. Stress–strain curves of chitin and chitin–HNTs hybrid hydrogels.

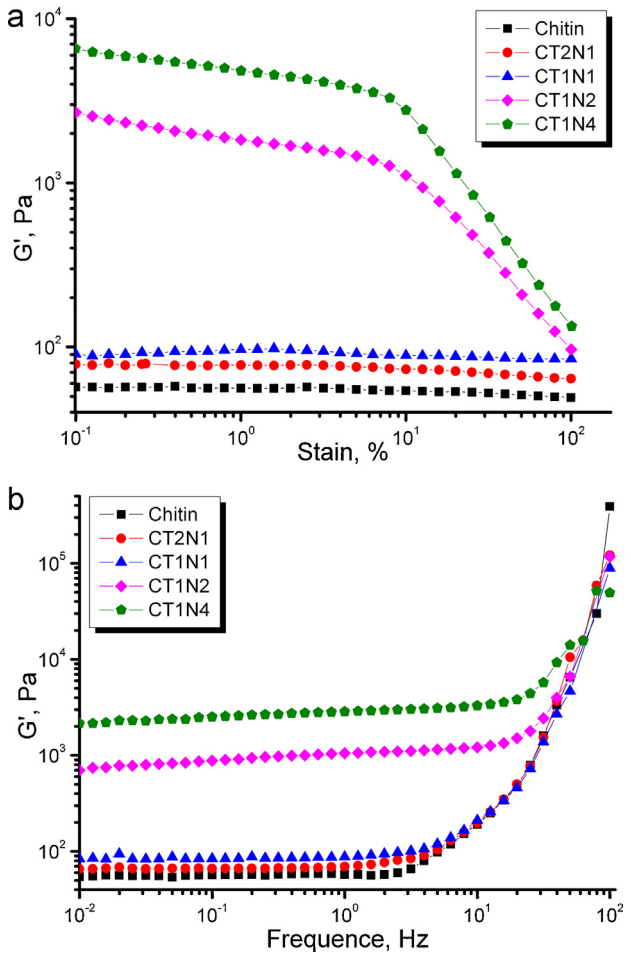

Fig. 5. Strain (a) and angular frequency (b) dependence of storage modulus G′ at 25 °C for chitin and chitin–HNTs hybrid hydrogels.

soft but tight polymer network and the rigid but loose inorganic network. The polymer network is formed by the crosslinked chitin chains with ECH and physical entanglement of molecular chains, while the inorganic network is formed via the hydrogen bonding interactions among the tubes. Upon loading, the relative loose inorganic networks can be seriously destroyed by the stress. So the shear modulus decreases sharply for the hybrid hydrogel in high strain areas. The formation of filler networks in polymer matrix was also found in other systems [25,26]. In polyacrylamide nanocomposite hydrogel system with HNTs, a similar decreasing trend of the shear modulus with strain was also found [27].

The frequency sweeping results also demonstrate the reinforcing effect of HNTs on chitin hydrogel. Fig. 5(b) depicts angular frequency dependence of the shear modulus for chitin and chitin–HNTs hybrid hydrogels. Consistent with the G′ vs. strain curves, G′ for the chitin–HNTs hybrid hydrogels increases with the loading of HNTs at the frequency ranging from 0.001 to about 10 Hz. However, G' increases sharply for all the samples at relatively high frequencies and no difference for these samples can be identified. In high frequency region, only the mobility of bond length and bond angle of polymer chains can occur while the movement of the polymer chain segments cannot take place. As discussed above, HNTs mainly affect the network structures of polymers in the hybrid hydrogel. Therefore, the influence of HNTs on the shear modulus becomes weak at high frequency. In total, rheology results further reflect the excellent the reinforcing effect of HNTs for chitin hydrogels.

3.4. Microstructure of chitin–HNTs hybrid hydrogels

To understand the mechanical property and swelling behaviors of chitin–HNTs hybrid hydrogels, the microstructures of corresponding freeze-dried hydrogels were analyzed via SEM. SEM is a powerful tool to study the three-dimensional network structure of hydrogels. The SEM photos of cross-section of chtitin and chitin–HNTs dried gel are shown in Fig. 6. Both chitin and chitin–HNTs hydrogels exhibit large interconnected pores with pore size of 100–200 μm. The average pore sizes of chitin and chitin–HNTs hybrid hydrogel with low HNTs concentration are about 200 μm, while the pore wall is in several micrometers. With high HNTs concentration (CT1N4), the hybrid hydrogel exhibits reduced pore size, as a result of the decrease in water volume in the hydrogel. It is generally considered that the pore formation of the dried gels is a two-phase separation process between the polymer-rich phase and the polymer-lean phase during the cross-linking reaction. The polymers form a pore wall, and pore size depends on the diffusion rate and amount of non-solvent into the solidification region. The high concentration of HNTs in the hybrid hydrogel leads to increased crosslinking density and a fast phase separation process [28], which further results in smaller pores in the hydrogel networks. The pores in these hydrogels facilitate transport of not only nutrients and metabolites but also cell migration and proliferation, so the prepared chitin–HNTs hybrid hydrogels can be used as three-dimensional (3D) scaffolds for tissue engineering or as dye adsorbent.

3.5. Swelling Properties of chitin–HNTs hybrid hydrogels

To determine the effect of HNTs on the swelling properties of chitin hydrogel, swelling experiment for all the hydrogel samples was conducted. The as-prepared hydrogels were not fully swollen. To determine their swelling properties, the prepared hydrogels were soaked in a large amount of water. Fig. 7(a) compares the equilibrium swelling ratio (EDS) of the hydrogels. As shown in the figure, with the increase of HNTs concentration, EDS of the hydrogel samples decreases from 116.2 to 28. The pure chitin hydrogel has the highest equilibrium swelling ratio (116.2) and the value is comparable with the result of Zhang et al. [7]. The value means that the pure chitin hydrogel can absorb more than its equivalent amount of water. It is generally considered that the EDS of hydrogel depends on both the hydrophilicity of the polymer chains and the physical structure. The incorporation of HNTs into the hybrid hydrogels results in a decrease in the polymer ratio of the hydrogel. Since the water adsorption of the nanoclay is limited, it is considered that the water adsorption property of the polymer networks makes the main contribution to the water adsorption of the hydrogels. As a result, the decreased polymer component in the hybrid hydrogels leads to the decreased EDS. In addition, the increase in HNTs loading in the hybrid hyrogels leads to the increases in crosslinking density of polymers. The increased crosslink density makes the space among the network for water molecules smaller. Another important factor affecting the adsorption of water is the microstructure of the gel. From the SEM result above, the pure chitin hydrogel has relatively large pore size. After the addition of HNTs, the pore size of the hydrogel decreases especially at high HNTs loading, therefore, the EDS decreases. All in all, the chitin–HNTs hydrogels with different EDS can be obtained by adjusting the concentration of HNTs for various applications.

3.6. Absorption MG behavior of chitin–HNTs hybrid hydrogels

Most of organic dyestuffs are harmful to human beings and toxic to microorganisms, so removal of dyestuffs from waste

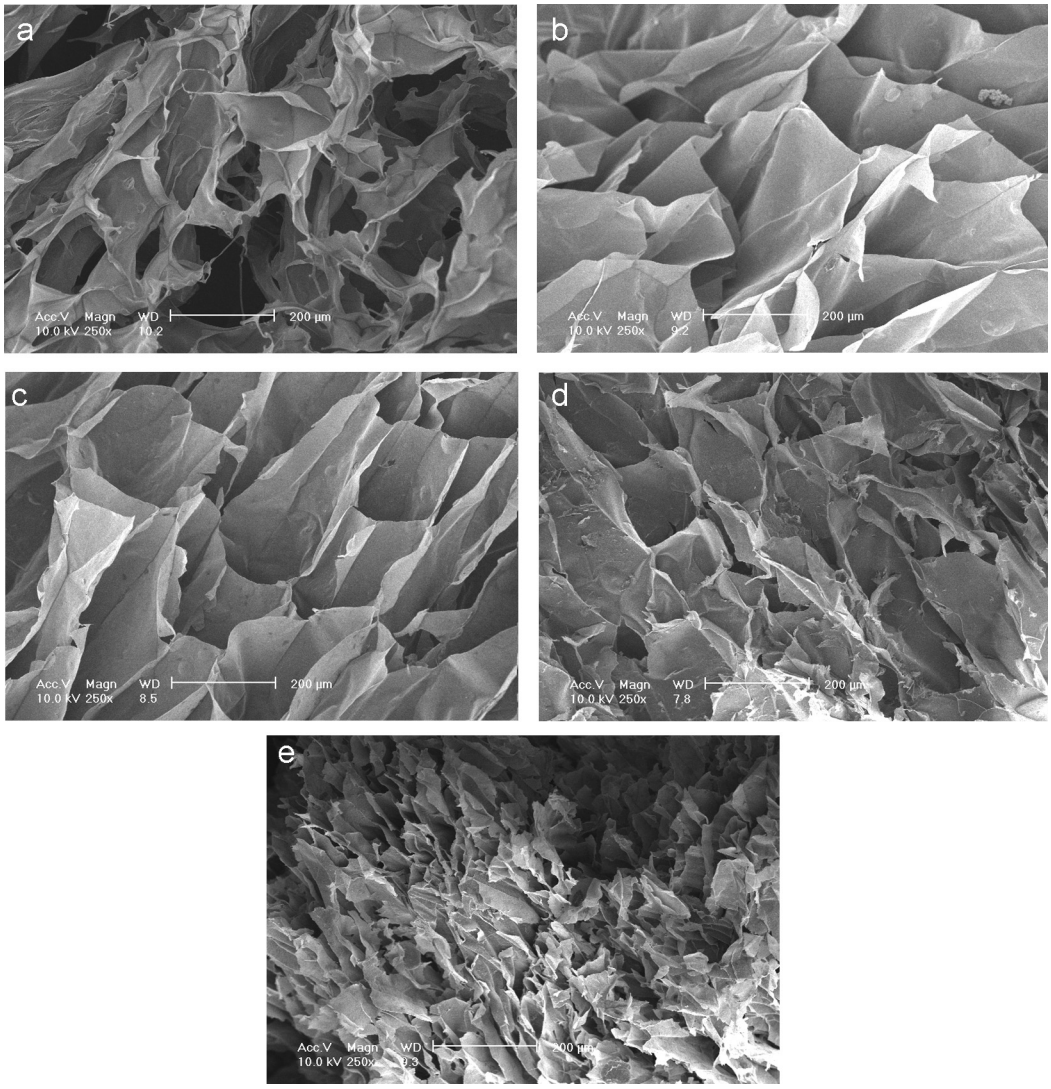

Fig. 6. SEM photos for freeze-dried chitin and chitin–HNTs hybrid hydrogels: (a) chitin; (b) CT2N1; (c) CT1N1; (d) CT1N2; (e) CT1N4.

water has received considerable attention. Polysaccharide based hydrogels can be used as the dyestuffs adsorbents for the waste water, since the porous network structures and the hydrophilic of the polymer chain make them having super high dye adsorption ability [29]. We took MG as the model dye to investigate the influence of HNTs on the absorption behavior of chitin hydrogel. The color changes of the MG solution before and after absorption by the chitin and chitin–HNTs hydrogel show the effect of HNTs on the absorption rate of the hydrogels to the dye (The photos can be seen in Supplementary 1). The dark blue of MG solution transfers into light blue or nearly colorless solution when increasing the HNTs concentration in the hybrid hydrogel after 24 h absorption. The pure chitin hydrogel has the slowest absorption rate from the color change of the solutions, while the CT1N4 hydrogel has the fastest absorption rate for MG among these samples. As early as 4 h after immersing of the CT1N4 hydrogel in MG solution, nearly all the MG molecules are absorbed on the hydrogel and the color of the solution turns into colorless. This indicates that HNTs have a very high promoting effect on the absorption of MG in the solutions. This can be attributed to the strong interaction between the dyestuffs and the clays [30,31]. With the absorption time increasing, the color further becomes light for all the samples. And after about 10 days, all the solutions turn into colorless. Therefore, it can be concluded that compared with the pure chitin hydrogel the hybrid hydrogel exhibits a significant increase in absorption efficiency. The combination effect of the hydrogel's macropore-structure and HNTs' unique properties is responsible for the significant improvement in dye absorption performance.

Fig. 7(b) shows the dependence of the q_e value of chitin and chitin–HNTs hydrogel versus the contact time. The q_e slowly increases for pure chitin hydrogel. In contrast, for the hybrid hydrogel especially at high HNTs concentration, the q_e increases rapidly in the initial stages. And with the increase of contact time, the q_e then gradually increased until adsorption equilibrium. The absorption equilibrium time of MG for CT, CT2N1, CT1N1, CT1N2, CT1N4 sample is 144 h, 72 h, 72 h, 48 h, and 24 h respectively. It can also be seen the incorporation of HNTs into chitin significantly increases the absorption rate for MG. Beside, it also should be noted that the price of HNTs is much lower than that of chitin, so the incorporation of HNTs into chitin leads to a decrease in the cost of the materials. Therefore, the enhanced mechanical properties, accelerated absorption rate and the lower price of the chitin–HNTs hybrid hydrogels are good for their practical applications in waste water treatment and biomaterials areas.

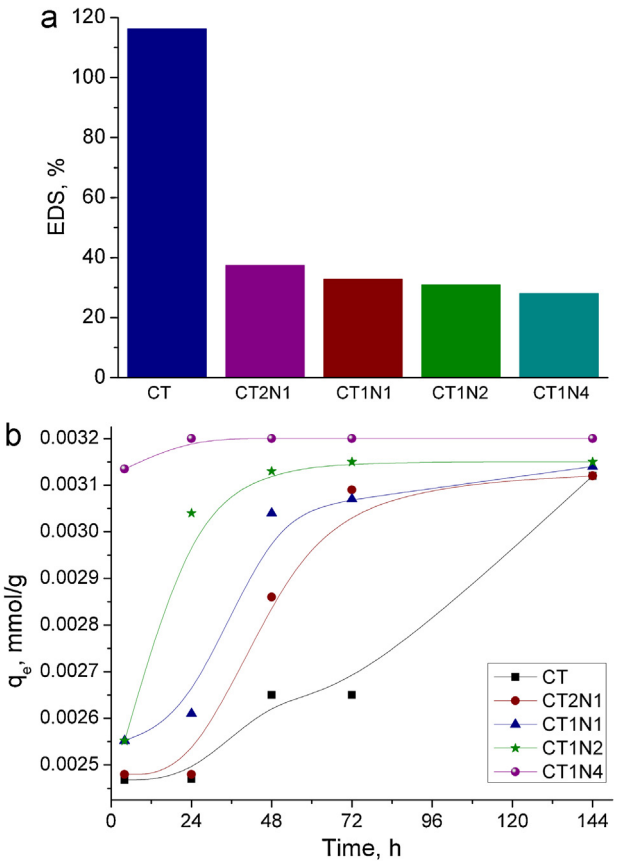

Fig. 7. The equilibrium swelling ratio (a) and MG adsorption behavior (b) of chitin and chitin–HNTs hybrid hydrogels.

4. Conclusions

The chitin–HNTs hybrid hydrogels were successfully prepared by solution mixing and subsequently crosslinking with ECH. The covalent bond and hydrogen bond interactions between HNTs and chitin were confirmed. The maximum compressive strength of the chitin–HNTs was ~60 kPa, which was ~300% higher than that of pure chitin hydrogel. The shear modulus of the hybrid hydrogel was also higher than that of pure chitin hydrogel in different frequencies and strains. Both chitin and chitin–HNTs dried gels exhibited highly porous structure with thin pore walls. The swelling ability of the hybrid hydrogel decreased compared with pure chitin hydrogel. HNTs had a promoting effect on the absorption of malachite green in their aqueous solutions. The absorption equilibrium time was largely shortened by the incorporation of HNTs. Due to the increased mechanical properties, the improved absorption ability, and lowered cost of chitin–HNTs hybrid hydrogel, they had potential applications in waste water treatment and biomaterials areas.

Acknowledgements

This work was financially supported by the Research Fund for the Doctoral Program of Higher Education of China (grant No. 20114401120003), the Key project of department of education of Guangdong province (No. cxzd1108), Key Laboratory of Rubber-plastics (Qingdao University of Science and Technology), Ministry of Education and the Key Laboratory of High Performance and Functional Polymeric Materials (South China University of Technology), Guangdong province, PR of China. The authors also thank Dr. Hau-To Wong for reading and revising of the manuscript.

Appendix A. Supplementary data

Supplementary data associated with this article can be found, in the online version, at http://dx.doi.org/10.1016/j.ijbiomac.2013.03.042.

References

[1] E. Khor, L.Y. Lim, Biomaterials 24 (2003) 2339–2349.
[2] M.N.V. Ravi Kumar, Reactive and Functional Polymers 46 (2000) 1–27.
[3] M. Rinaudo, Progress in Polymer Science 31 (2006) 603–632.
[4] C.K.S. Pillai, W. Paul, C.P. Sharma, Progress in Polymer Science 34 (2009) 641–678.
[5] P.K. Dutta, J. Dutta, V.S. Tripathi, Journal of Scientific & Industrial Research 63 (2004) 20–31.
[6] X. Hu, Y. Du, Y. Tang, Q. Wang, T. Feng, J. Yang, J.F. Kennedy, Carbohydrate Polymers 70 (2007) 451–458.
[7] C. Chang, S. Chen, L. Zhang, Journal of Materials Chemistry 21 (2011) 3865–3871.
[8] B. Ding, J. Cai, J. Huang, L. Zhang, Y. Chen, X. Shi, Y. Du, S. Kuga, Journal of Materials Chemistry 22 (2012) 5801–5809.
[9] F. Chivrac, E. Pollet, L. Averous, Materials Science and Engineering: R: Reports 67 (2009) 1–17.
[10] C. Chang, N. Peng, M. He, Y. Teramoto, Y. Nishio, L. Zhang, Carbohydrate Polymers 91 (2012) 7–13.
[11] E. Joussein, S. Petit, J. Churchman, B. Theng, D. Righi, B. Delvaux, Clay Minerals 40 (2005) 383–426.
[12] M.X. Liu, B.C. Guo, M.L. Du, X.J. Cai, D.M. Jia, Nanotechnology 18 (2007) 455703.
[13] M. Du, B. Guo, D. Jia, Polymer International 59 (2010) 574–582.
[14] M. Liu, B. Guo, M. Du, D. Jia, Applied Physics A: Materials Science and Processing 88 (2007) 391–395.
[15] M. Liu, Y. Zhang, C. Wu, S. Xiong, C. Zhou, International Journal of Biological Macromolecules 51 (2012) 566–575.
[16] G. Cavallaro, G. Lazzara, S. Milioto, Langmuir 27 (2011) 1158–1167.
[17] Y.M. Lvov, D.G. Shchukin, H. Mohwald, R.R. Price, Acs Nano 2 (2008) 814–820.
[18] S. Kinugasa, K. Tanabe, T. Tamura, in, National Institute of Advanced Industrial Science and Technology (AIST), Japan.
[19] R. Zhou, M. Xu, Z. An, Chinese Journal of Liquid Crystals and Displays 25 (2010) 172–175.
[20] P. Podsiadlo, A.K. Kaushik, E.M. Arruda, A.M. Waas, B.S. Shim, J.D. Xu, H. Nandivada, B.G. Pumplin, J. Lahann, A. Ramamoorthy, N.A. Kotov, Science 318 (2007) 80–83.
[21] J.B. Han, Y.B. Dou, D.P. Yan, J. Ma, M. Wei, D.G. Evans, X. Duan, Chemical Communications 47 (2011) 5274–5276.
[22] J.D. Schiffman, C.L. Schauer, Biomacromolecules 8 (2007) 594–601.
[23] K. Haraguchi, Polymer Journal 43 (2011) 223–241.
[24] A. Okada, A. Usuki, Macromolecular Materials and Engineering 291 (2006) 1449–1476.
[25] P.J. Fu, K.L. Xu, H.Z. Song, G.M. Chen, J.P. Yang, Y.H. Niu, Journal of Materials Chemistry 20 (2010) 3869–3876.
[26] R. Krishnamoorti, E.P. Giannelis, Macromolecules 30 (1997) 4097–4102.
[27] M. Liu, W. Li, J. Rong, C. Zhou, Colloid and Polymer Science 290 (2012) 895–905.
[28] S.G. Levesque, R.M. Lim, M.S. Shoichet, Biomaterials 26 (2005) 7436–7446.
[29] G. Crini, Progress in Polymer Science 30 (2005) 38–70.
[30] M. Zhao, P. Liu, Microporous and Mesoporous Materials 112 (2008) 419–424.
[31] M.X. Liu, B.C. Guo, Q.L. Zou, M.L. Du, D. Jia, Nanotechnology 19 (2008) 205709.